MBoC | ARTICLE

Modulation of receptor dynamics by the regulator of G protein signaling Sst2

Sai Phanindra Venkatapurapu[a,*], Joshua B. Kelley[b,c,*], Gauri Dixit[b], Matthew Pena[c], Beverly Errede[b], Henrik G. Dohlman[b,c], and Timothy C. Elston[a,c]

[a]Curriculum in Bioinformatics and Computational Biology, [b]Department of Biochemistry and Biophysics, and [c]Department of Pharmacology, University of North Carolina at Chapel Hill, Chapel Hill, NC 27599

ABSTRACT **G protein–coupled receptor (GPCR) signaling is fundamental to physiological processes such as vision, the immune response, and wound healing. In the budding yeast *Saccharomyces cerevisiae*, GPCRs detect and respond to gradients of pheromone during mating. After pheromone stimulation, the GPCR Ste2 is removed from the cell membrane, and new receptors are delivered to the growing edge. The regulator of G protein signaling (RGS) protein Sst2 acts by accelerating GTP hydrolysis and facilitating pathway desensitization. Sst2 is also known to interact with the receptor Ste2. Here we show that Sst2 is required for proper receptor recovery at the growing edge of pheromone-stimulated cells. Mathematical modeling suggested pheromone-induced synthesis of Sst2 together with its interaction with the receptor function to reestablish a receptor pool at the site of polarized growth. To validate the model, we used targeted genetic perturbations to selectively disrupt key properties of Sst2 and its induction by pheromone. Together our results reveal that a regulator of G protein signaling can also regulate the G protein–coupled receptor. Whereas Sst2 negatively regulates G protein signaling, it acts in a positive manner to promote receptor retention at the growing edge.**

Monitoring Editor
Leah Edelstein-Keshet
University of British Columbia

Received: Dec 22, 2014
Revised: Aug 12, 2015
Accepted: Aug 13, 2015

INTRODUCTION

Heterotrimeric G proteins are molecular switches that are activated by ligand-bound receptors at the cell surface (Sprang, 1997). Regulators of G protein signaling (RGS) proteins dampen signaling by accelerating the GTPase activity of heterotrimeric G proteins. Recently RGS proteins have received attention as potential drug targets for treating diseases ranging from heart disease to neurological disorders (Neubig and Siderovski, 2002; Sjögren *et al.*, 2010; Zhang and Mende, 2011). Therefore a better understanding of the role of RGS proteins in signal transduction may facilitate the development of therapeutic treatments. In addition to their ability to accelerate GTPase activity, RGS proteins interact directly with G protein–coupled receptors (GPCRs; Hague *et al.*, 2005; Kovoor *et al.*, 2005; Ballon *et al.*, 2006). This interaction with the receptor presumably enhances the activity of the RGS protein toward the Gα subunit (Ballon *et al.*, 2006). However, the effects of these interactions on GPCR function have not been fully characterized. Therefore we turned to the yeast RGS protein Sst2 to further elucidate the role of these proteins in GPCR signaling. Sst2 is the founding member of the RGS protein family.

The yeast pheromone pathway provides an excellent model system for characterizing G protein–mediated signaling. Yeast can exist stably as diploids or as one of two haploid mating types (Dohlman and Thorner, 2001). To find a mating partner, haploid yeast detect and respond to gradients of pheromone secreted by cells of the opposite mating type (Segall, 1993). The response to pheromone is mediated by a GPCR (Ste2; Dohlman and Thorner, 2001). Before pheromone stimulation, the GPCR is bound to a heterotrimeric G protein composed of an α-subunit, Gpa1, and a βγ-heterodimer, Ste4/Ste18. On pheromone binding to the receptor, Gα releases

This article was published online ahead of print in MBoC in Press (http://www.molbiolcell.org/cgi/doi/10.1091/mbc.E14-12-1635) on August 26, 2015.

*These authors contributed equally to this work.

The authors declare that they have no conflict of interest.

Address correspondence to: Timothy Elston (timothy_elston@med.unc.edu), Henrik Dohlman (henrik_dohlman@med.unc.edu).

Abbreviations used: DEP, Dishevelled, Egl-10, and pleckstrin; DIC, differential interference contrast; GAP, GTPase-activating protein; GDP, guanosine diphosphate; GFP, green fluorescent protein; GPCR, G protein–coupled receptor; GTP, guanosine triphosphate; MAPK, mitogen-activated protein kinase; ODE, ordinary differential equation; RGS, regulator of G protein signaling; ROI, region of interest; SEM, standard error of the mean; WT, wild type.

Gβγ, which activates Cdc42 and promotes cell polarization. A second branch of the pathway initiates a mitogen-activated protein kinase (MAPK) cascade that leads to new gene transcription (Dohlman and Thorner, 2001), which includes induced expression of the RGS protein Sst2. Sst2 acts as a GTPase-activating protein (GAP), enhancing the rate of Gα-catalyzed GTP hydrolysis (Dohlman *et al.*, 1996; Apanovitch *et al.*, 1998). GDP-bound Gα rapidly reassociates with Gβγ, terminating the pheromone response. Thus Ste2 is required for signal transmission, whereas Sst2 is required for signal termination and pathway desensitization.

It is well established that pheromone receptors are delivered to the cell surface via the secretory pathway but are later internalized and delivered to the vacuole for degradation. Both processes are accelerated by pheromone stimulation (Jenness and Spatrick, 1986). Endocytosis requires that receptors be phosphorylated in the C-terminal "tail" domain (Reneke *et al.*, 1988; Chen and Konopka, 1996). Mutations in the Ser and Thr residues within the tail or removal of the tail entirely result in a loss of ligand-induced endocytosis and increased sensitivity to α-factor (Konopka *et al.*, 1988; Reneke *et al.*, 1988; Chen and Konopka, 1996). Surprisingly, receptor down-regulation occurs even in mutant cells that lack an active G protein (Jenness and Spatrick, 1986; Zanolari *et al.*, 1992). Similarly, a receptor mutant that is defective in transmitting the pheromone signal is still capable of undergoing ligand-dependent endocytosis (Schandel and Jenness, 1994). Thus G protein–mediated signal transduction is not necessary for Ste2 phosphorylation or internalization. Based on these observations, it is generally accepted that α-factor binding induces a conformational change in the receptor, thereby increasing its accessibility for both phosphorylation and interaction with the endocytic machinery.

In addition to an RGS domain, which performs the GAP function, Sst2 possesses a Dishevelled, Egl-10, and pleckstrin (DEP) domain, which interacts with the receptor Ste2 (Ballon *et al.*, 2006). Of interest, the phosphorylation sites on Ste2 overlap with the binding site for Sst2 (Ballon *et al.*, 2006; Suchkov *et al.*, 2010), suggesting that Sst2 interaction with the receptor might influence receptor internalization. Thus Sst2 interaction with Ste2 would represent a point of convergence at which one desensitization mechanism in the pheromone pathway (Sst2 GAP activity) interacts with another desensitization mechanism in the same pathway (receptor internalization).

Recent advances in live-cell imaging and computational image analysis have generated new insights into many aspects of cell signaling. In yeast, these new tools have been combined with mathematical modeling to investigate dose alignment (Yu *et al.*, 2008), noise regulation (Dixit *et al.*, 2014), cell fate decisions (Doncic *et al.*, 2011), and gradient sensing (Hao *et al.*, 2008; Jin *et al.*, 2011; Howell *et al.*, 2012; Dyer *et al.*, 2013; Kelley *et al.*, 2015). The success of these investigations motivated us to apply a similar approach to investigate Sst2's role in regulating receptor endocytosis. As described later, we developed a computational model that captures the dynamics of pheromone-dependent receptor internalization and subsequent delivery of newly synthesized receptor to the cell membrane. Using targeted genetic perturbations, we showed that the model successfully predicts the response of cells in which the two functions of Sst2 are selectively disrupted. Our investigations also demonstrated that Sst2's interaction with the receptor, and not its GAP activity, is necessary for proper localization of the receptor. Unexpectedly, the model suggested that Sst2 induction is required for proper receptor localization, a prediction we confirmed experimentally. These findings reveal a new function for RGS proteins in receptor trafficking and illustrate the utility of predictive computational models in cell signaling research.

RESULTS

Pheromone-induced endocytosis and recovery of Ste2 is dose dependent

It is well established that receptor phosphorylation leads to endocytosis and delivery to the vacuole. Sst2 binds preferentially to the unphosphorylated form of the receptor Ste2, but the functional consequences of this interaction have not been established. Therefore we sought to determine whether Sst2 plays a role in regulating the time-dependent localization of receptors after pheromone stimulation. To that end, we first characterized receptor dynamics in wild-type cells using live-cell imaging and yeast expressing an Ste2–green fluorescent protein (GFP) fusion protein. The yeast were maintained in a uniform pheromone concentration within a microfluidic device, as we used previously (Hao *et al.*, 2008; Dixit *et al.*, 2014; Kelley *et al.*, 2015; Figure 1A). We next quantified changes in membrane-bound receptor over time using the method illustrated in Figure 1B. Briefly, we created a region of interest three pixels wide encompassing the plasma membrane and measured the fluorescence intensity within the region. As shown in Figure 1C (all individual cell data are given in Supplemental Figure S1), we observed an initial decrease in membrane-bound Ste2-GFP when wild-type cells were treated with a saturating concentration (150 nM) of pheromone. This yeast strain, BY4741, expresses the pheromone protease Bar1, increasing the amount of pheromone required to elicit a response. After 40 min, newly synthesized receptor began to appear at the plasma membrane. This new pool of receptor was distributed in a polarized manner, consistent with previous observations (Suchkov *et al.*, 2010; Figure 1A). At a lower dose of pheromone closer to the dissociation constant (10 nM), the membrane-bound receptor pool did not decrease and instead remained constant until ~60 min, at which point, receptor levels on the plasma membrane began increasing (Figure 1, A and C). From these data, we conclude that the dynamics of receptor trafficking during the pheromone response is dose dependent.

At both pheromone concentrations, Ste2 eventually became polarized at the growing edge. The level of receptor accumulation was higher when cells were exposed to a lower dose of pheromone. This led us to ask whether the different levels of receptor were also localized differently. To best answer this question, we implemented a quantitative method for determining the receptor distribution (Kelley *et al.*, 2015). The average receptor distribution was calculated by first smoothing fluorescence measurements made from individual cells and then aligning the distributions using the maximum values of the smoothed data (Supplemental Figure S2). Once the individual cell distributions were aligned, the raw data were averaged. We found that at the higher pheromone dose of 150 nM, the receptor distribution was sharper than at the low, 10 nM dose (Figure 1D). This difference may be attributable to the slower rate at which the receptor becomes occupied when exposed to lower concentrations of pheromone, thereby allowing the receptor to diffuse further before it becomes internalized. Thus our results demonstrate that receptor internalization, receptor recovery, and receptor distribution on the plasma membrane are dose dependent.

Pheromone-induced endocytosis and recovery of Ste2 is regulated by Sst2

RGS proteins attenuate signaling by binding to the Gα subunit of heterotrimeric G proteins and inducing the hydrolysis of GTP. In addition to acting as GAPs, Sst2 and other RGS proteins have been shown to bind directly to GPCRs. Moreover, the Sst2-binding site on Ste2 overlaps with the phosphorylation sites necessary to drive receptor internalization (Ballon *et al.*, 2006). These observations led us

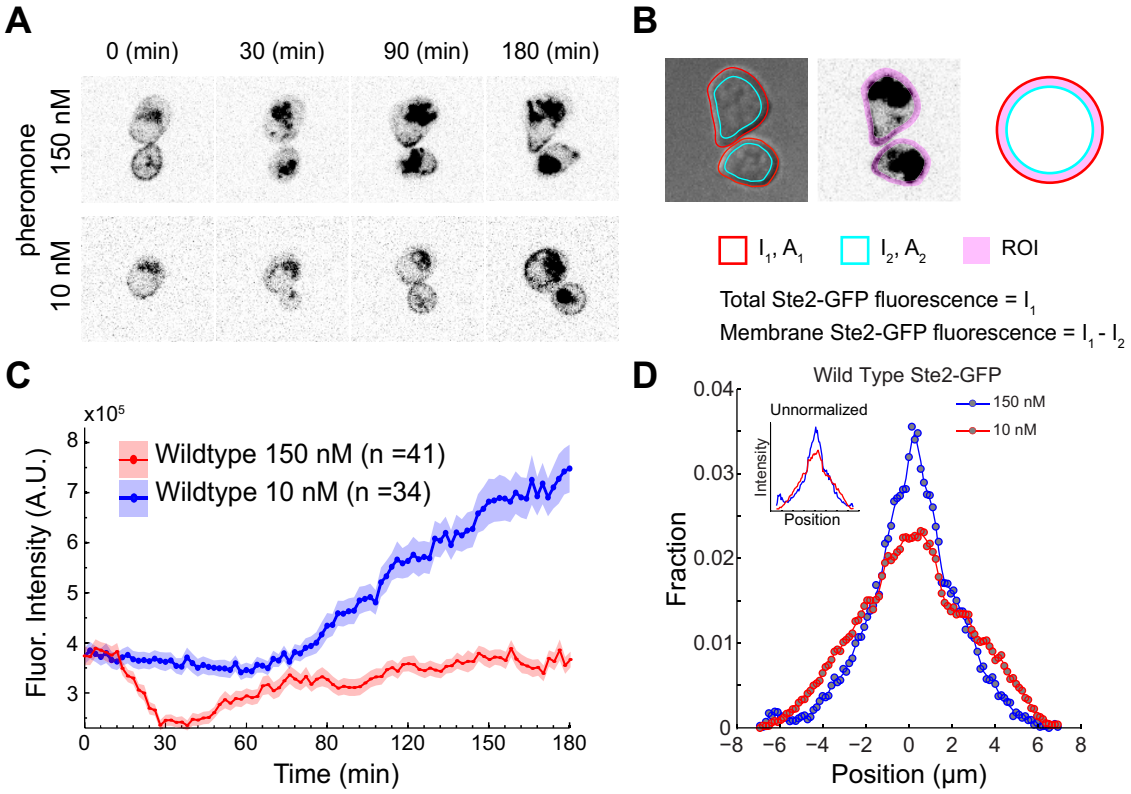

FIGURE 1: Sst2 regulates pheromone-dependent endocytosis and receptor recovery. (A) Representative fluorescence images of Ste2-GFP in WT cells treated with 150 nM (top) and 10 nM (bottom) pheromone. (B) Quantification of membrane-bound Ste2-GFP from fluorescence microscopy data. Cell boundaries (red circles) were identified manually and saved in ImageJ ROI Manager. The cell boundary (red circle) was shrunk by three pixels (cyan circle) to create an annular ring around the cell membrane (region of interest [ROI], pink). Fluorescence intensity in the annular ring is a measure of Ste2-GFP on the cell membrane. Fluorescence intensity inside the red circle is a measure of Ste2-GFP in the cell as a whole. (C) Membrane-bound Ste2-GFP fluorescence plotted as a function of time in WT cells exposed to 10 or 150 nM pheromone. Solid lines represent the mean and shaded regions the SEM. (D) Spatial distribution of receptor in high (150 nM) and low (10 nM) pheromone. Distributions from individual cells were aligned so that peak fluorescence is located at 0 μm and normalized such that the area under the curve is 1. The individual distributions were then averaged to produce the results shown. Inset, unnormalized profiles at high and low pheromone.

to hypothesize that Sst2's interaction with Ste2 could have significant consequences for the spatiotemporal dynamics of the receptor. To test this possibility, we monitored Ste2-GFP fluorescence in cells lacking Sst2 (*sst2*Δ; Figure 2A). To compare results between wild-type and *sst2*Δ experiments, we measured unstimulated Ste2 levels in wild-type cells and the *sst2*Δ strain in a single experiment (Figure 2B; note that in this experiment, we also measured Ste2 levels for all the strains used in these investigations; see *Materials and Methods* for details). These measurements allowed us to normalize all fluorescence data relative to wild-type (WT) cells. This normalization adjusts for differences in illumination and other day-to-day variation between experiments performed in our microfluidics chamber (Dixit *et al.*, 2014). Before pheromone treatment, there was less Ste2-GFP at the plasma membrane of *sst2*Δ mutants than with wild-type cells (Figure 2B). Thus expression of Sst2 lowers the baseline concentration of receptor on the membrane.

Next we monitored the time-dependent behavior of membrane-bound receptor. At high pheromone concentration, receptor levels at the plasma membrane decreased in both *sst2*Δ and wild-type cells (Figure 2C). At later times, however, membrane-bound receptor levels increased in wild-type cells, whereas receptor levels remained relatively flat in *sst2*Δ cells. At low pheromone concentration, receptor levels at the plasma membrane did not decrease significantly in either *sst2*Δ or wild-type cells. At later times, receptor levels increased above basal levels in both strains, although *sst2*Δ cells showed a modest increase of membrane receptor levels over time in comparison to wild-type cells (Figure 2D). These results demonstrate that Sst2 is required for recovery of receptor to the plasma membrane after pheromone stimulation.

Sst2 affects receptor distribution but not its pheromone-induced expression

Transcription of the receptor is induced by pheromone stimulation (Jenness and Spatrick, 1986), and it is possible that alterations in gene regulation underlie the defect in receptor recovery observed in the *sst2*Δ strain. To rule out this possibility, we monitored cumulative receptor induction over time in WT cells and in cells lacking Sst2. After internalization, the receptor Ste2 is degraded in vacuoles (Jenness and Spatrick, 1986). However, GFP is resistant to proteolysis in the vacuole (Shintani and Klionsky, 2004), and thus total cellular GFP fluorescence is an indicator of cumulative Ste2 production. Measurements of total GFP fluorescence in WT and *sst2*Δ cells revealed that Ste2 levels increase in both cell types to roughly the same amount after pheromone treatment (Figure 2E). The observation that

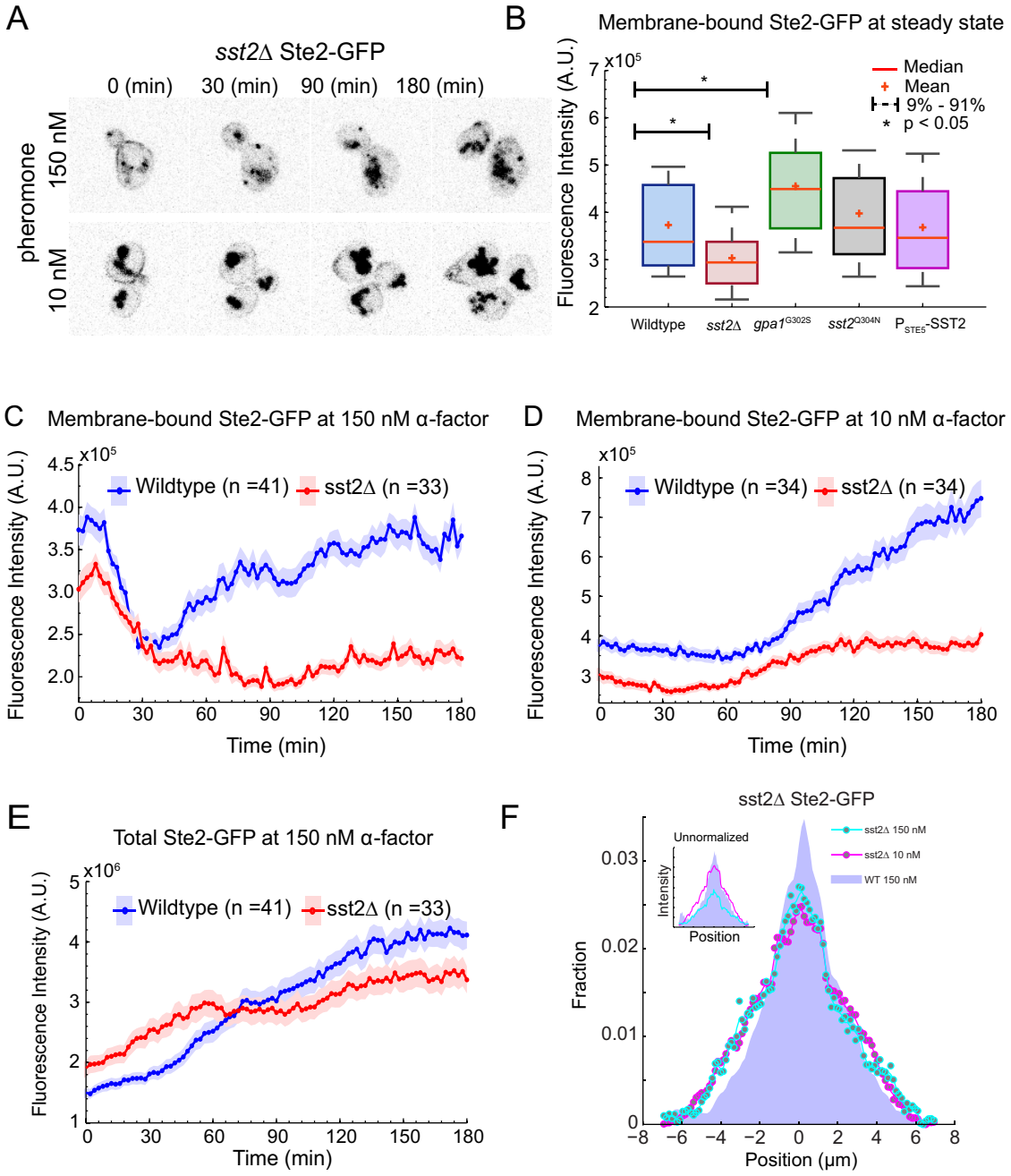

FIGURE 2: Ste2 levels are regulated by Sst2. (A) Representative fluorescence images of Ste2-GFP in *sst2*Δ cells treated with 150 nM (top) and 10 nM (bottom) pheromone. (B) Box-and-whisker plot of membrane-bound Ste2-GFP fluorescence in untreated cells. Each box represents lower quartile (25%) to upper quartile (75%) of the data. Whiskers (broken lines) represent values outside the upper and lower quartiles. Ends of the whiskers (solid black lines) represent 9th and 91st percentiles. Red bars represent the medians of the data, and the plus signs represent the means. (C) Membrane-bound Ste2-GFP fluorescence plotted as a function of time in WT and *sst2*Δ cells exposed to 150 nM pheromone. Solid lines represent the mean and shaded regions the SE in the data. (D) As in C, but cells were exposed to 10 nM pheromone. (E) Total Ste2-GFP fluorescence in WT and *sst2*Δ cells as a function of time. Solid lines represent the mean and shaded areas the SE in the data. Cells were treated with 150 nM pheromone starting at 0 min. (F) Spatial distributions of receptor in *sst2*Δ cells at high (150 nM) and low (10 nM) pheromone, as in Figure 1D. Inset, unnormalized profiles of WT and *sst2*Δ at high pheromone.

*sst2*Δ cells show somewhat diminished Ste2 levels at later times, even though these cells are more sensitive to pheromone, might be attributed to *sst2*Δ cells having fewer membrane-bound receptors through which to signal. Despite equivalent levels of overall expression in WT and *sst2*Δ cells, significant levels of Ste2 were detected at the plasma membrane only in WT cells. We conclude that Sst2 ensures proper retention of Ste2 at the plasma membrane by mechanisms other than by regulating receptor synthesis.

Because Sst2 is required for proper accumulation of receptor at the plasma membrane, we sought to determine whether Sst2 also

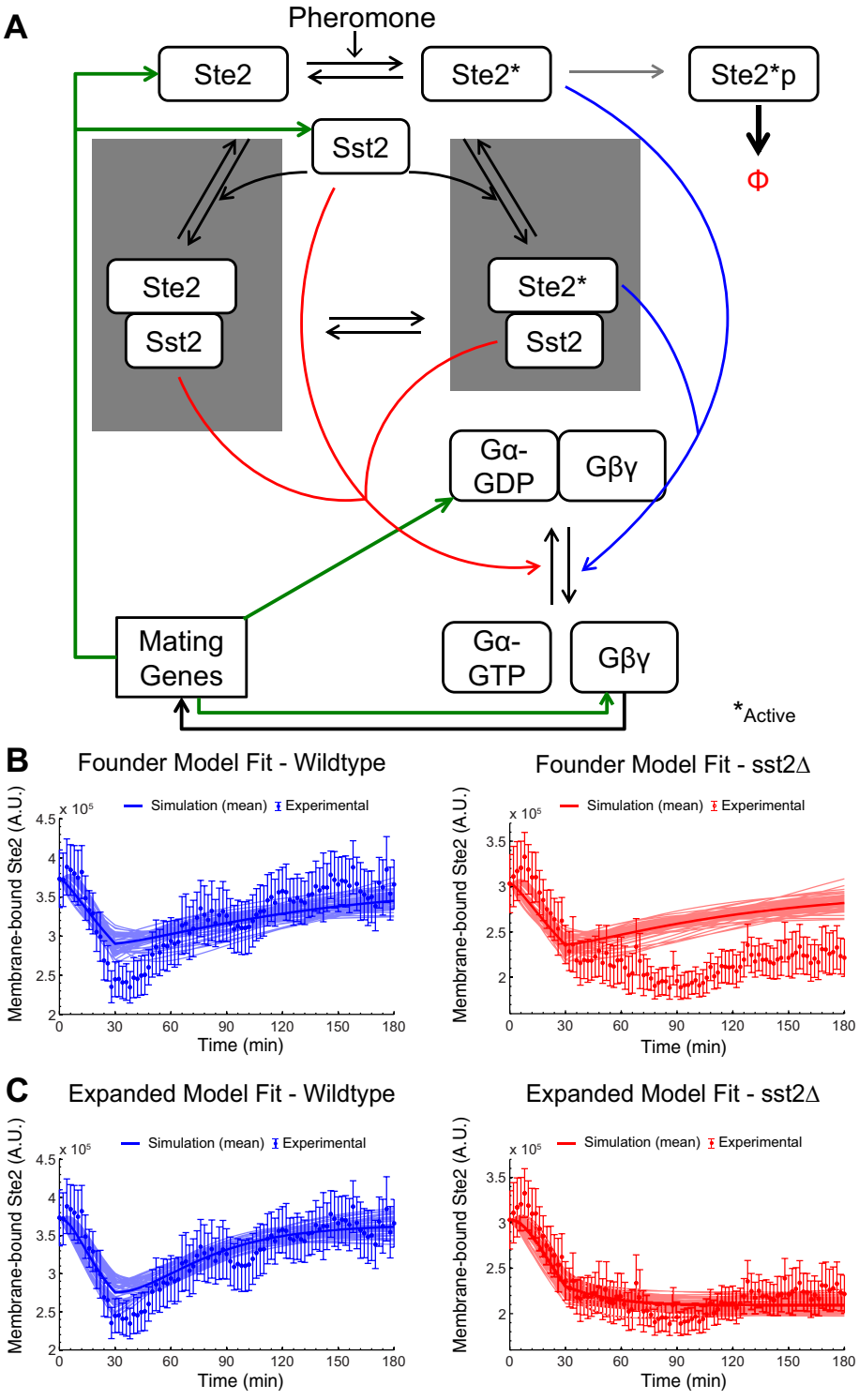

FIGURE 3: Computational modeling predicts Sst2's role in regulating receptor endocytosis. (A) Diagram showing the founder and expanded models of receptor endocytosis. Double black arrows represent reversible reactions involving ligand–receptor and protein–protein interactions. Dark blue arrows represent guanine nucleotide exchange activity of the receptor, and red arrows represent GAP activity of Sst2. Green arrows represent pheromone-dependent gene expression. The light gray arrow represents receptor phosphorylation, and the bold black arrow represents endocytosis of phosphorylated receptor. Reaction modules shown in gray boxes were added to the founder model to take into account Sst2's interaction with the receptor. (B) Model results for the founder model. The model was fit to Ste2-GFP fluorescence data for WT (left) and *sst2*Δ (right) cells under high-pheromone conditions. Simulation results from the 50 best parameter sets are shown as light solid curves. The bold solid curves represent the mean of the top 50 time series. The data points represent the mean experimental Ste2-GFP fluorescence, and the error bars represent 95% confidence intervals. (C) Model results for the expanded model. The same procedure as described in B was used to generate these results, except that the shaded interactions shown in A were added to the model.

affects receptor distribution. To measure the receptor profile in *sst2*Δ cells, we used the same approach as before for WT cells. Of interest, our analysis revealed that, in addition to increasing the amount of polarized receptor (Figure 2F, inset), Sst2 acts to sharpen the receptor distribution at high pheromone concentration (150 nM; Figure 2F). Thus Sst2, which is required for gradient tracking, may help to anchor the receptor at the leading edge of the cell in the direction of the gradient stimulus.

Computational modeling predicts Sst2's role in regulating receptor endocytosis

Our foregoing results demonstrate that, after pheromone stimulation, Sst2 is required for proper accumulation of the receptor on the plasma membrane. Our working hypothesis is that Sst2 regulates receptor accumulation at the plasma membrane by binding directly to the receptor and blocking its endocytosis. However, it is possible that the GAP activity of Sst2 plays a role in stabilizing receptor at the membrane, as suggested for RGS proteins in neurons (Celver *et al.*, 2010). Therefore, to identify potential mechanisms that could account for our data, we turned to mathematical modeling. The starting point for our investigation was the mathematical model of G protein signaling in the yeast mating response developed by Yildirim *et al.* (2004). We refer to this model as the "founder model" because it does not take into account Sst2's interaction with the receptor (this was not known at the time; Figure 3A). In this model, pheromone binding stimulates the transition of the receptor Ste2 to the activated form, Ste2*. The activated receptor Ste2* is then phosphorylated (Ste2*p), and the phosphorylated form of the receptor is available for internalization. Active receptor, Ste2*, promotes exchange of GDP to GTP on the Gα subunit Gpa1. GTP-bound Gpa1 (active form) dissociates from Gβγ, resulting in free Gβγ, which transduces the signal downstream. A downstream target of the pathway is the transcription factor Ste12, the activation of which leads to induced expression of the receptor Ste2 (positive feedback) and the RGS protein Sst2 (negative feedback). The model

assumes that free Gβγ determines the rate of gene induction without explicitly taking into account the activation of Ste12. Finally, the rate of G protein inactivation depends on the Sst2 level.

We used the founder model to test whether Sst2's GAP activity is sufficient to explain our experimental results. The behavior of any mathematical model depends on the parameter values used to define it. Thus, rather than trying to determine a single set of parameter values that produce the best fit of the model to the data, we implemented a Monte Carlo–based evolutionary algorithm to perform parameter estimation. This method produces sets of parameter values that yield fits to the data that are roughly equivalent to one another. We used the normalized time series for WT and *sst2*Δ cells as training sets to evaluate the model and perform parameter estimation. Based on this approach, the model successfully captured both the endocytosis and recovery behaviors of Ste2 in WT cells (Figure 3B). However, the model failed to capture the requirement for Sst2 expression in receptor recovery (Figure 3B). This discrepancy indicated that a second (non-GAP) function of Sst2 is needed to stabilize receptors at the membrane.

We then considered a mechanism in which Sst2 impedes phosphorylation of the receptor and inhibits its endocytosis. To that end, we expanded our founder model to include Sst2 interaction with the receptor (Figure 3A). In the "expanded" model (gray boxes), the receptor can exist in three states: inactive (Ste2), active (Ste2*), and active and phosphorylated (Ste2*p). Sst2 binds to both the inactive (Ste2) and active (Ste2*) forms of the receptor but not the phosphorylated form (Ste2*p). Binding of Sst2 prevents the active form Ste2* from becoming phosphorylated. Ste2 and Ste2* are internalized at a basal rate that is slower than the internalization rate of Ste2*p (see the Supplemental Information for model equations). We again used the Monte Carlo method to train the expanded model. The expanded model captured both the initial internalization and receptor recovery phases of WT cells and captured the loss of receptor recovery in *sst2*Δ cells (Figure 3C). Thus our modeling results suggest that Sst2 interaction with the receptor is necessary to stabilize the receptor at the plasma membrane after pheromone treatment.

Loss of GAP activity of Sst2 enhances receptor polarization

The results of our modeling indicated an important role for Sst2 in receptor localization. To investigate the role of Sst2 GAP activity in receptor endocytosis, we ran simulations using our expanded model in which the parameter that describes Sst2's GAP activity was set to 0. Simulations were run using the 50 best parameter sets obtained from fitting the WT and *sst2*Δ data. In all cases, the model predicted that selectively blocking Sst2's GAP activity would lead to higher levels of free Gβγ and, thus, increased Ste2 synthesis and basal levels at the membrane. In addition, the model predicted increased receptor recovery in the GAP-deficient mutant after pheromone stimulation (Figure 4B).

Just as Sst2 GAP activity and receptor binding can be altered computationally by changing rate constants, these functions can be altered experimentally using standard yeast genetic methods. To that end, we tested our model through the replacement of the endogenous genes with well-characterized point mutants that selectively disrupt either Sst2 GAP activity or Sst2 binding to the receptor (DiBello *et al.*, 1998; Ballon *et al.*, 2006). To investigate the effect of Sst2's GAP activity, we used the point mutant $gpa1^{G302S}$, which prevents the Gα subunit from interacting with Sst2 (DiBello *et al.*, 1998). Consistent with the model (Figure 4B), the $gpa1^{G302S}$ mutant showed increased basal levels of the receptor and higher receptor recovery than that observed in WT cells (Figure 4C).

Sst2 interaction with Ste2 is required for proper receptor recovery

Next we used the model to investigate how Sst2's interaction with the receptor affects receptor accumulation at the plasma membrane. To this end, we ran simulations in which the rate constant for receptor–Sst2 binding was set to 0 and again used the 50 best parameter sets. In all cases, Sst2's interaction with Ste2 was necessary for receptor recovery (Figure 4D). In addition to interacting with Gα and Ste2, Sst2 interacts with multiple other signaling proteins, including the MAPK Fus3 (Parnell *et al.*, 2005; Yu *et al.*, 2008). Therefore the failure to recover Ste2 at the plasma membrane of *sst2*Δ cells could be an indirect consequence of perturbations in downstream signaling events. To test directly whether Sst2 binding inhibits receptor endocytosis, we used another point mutant, $sst2^{Q304N}$, which selectively disrupts the interaction between Sst2 and Ste2 (Ballon *et al.*, 2006). Similar to *sst2*Δ cells, and in contrast to $gpa1^{G302S}$, the $sst2^{Q304N}$ mutant did not show any recovery of the receptor (Figure 4E). These results were in very good agreement with model predictions (Figure 4D). Together these results demonstrate that Sst2's interaction with the receptor, but not its GAP activity or interactions with other binding partners, is necessary for receptor recovery at the plasma membrane after pheromone stimulation.

Sst2 induction is necessary for proper Ste2 recovery at the membrane

Sst2 expression is induced in response to pheromone, and it is typically assumed that this increase in Sst2 represents a negative feedback loop that leads to signal attenuation. To investigate the effect of this feedback loop on receptor recovery, we ran simulations in which pheromone-induced synthesis of Sst2 was abolished (in the model, this is accomplished by setting the maximum induced Sst2 synthesis rate equal to zero). Surprisingly, the model predicted that blocking pheromone-dependent induction of Sst2 would inhibit receptor recovery (Figure 4F). To test this prediction, we replaced the endogenous *SST2* promoter with a noninducible promoter from *STE5* (P_{STE5}; Flotho *et al.*, 2004). Under conditions that constitutively express Sst2, abundance of receptor on the membrane was comparable to that of untreated WT yeast (Figure 2B). In agreement with the model, cells containing P_{STE5}-*SST2* showed significantly less receptor recovery than the WT strain (Figure 4G). These results demonstrate that after pheromone stimulation, increased Sst2 levels act to promote receptor retention at the growing edge by blocking internalization of Ste2.

Sst2 as a noise regulator

It is well established that Sst2 promotes G protein GTPase activity and thereby dampens the activity of downstream effectors. More recently, we showed that Sst2 suppresses cell-to-cell variability (noise) in transcription and morphogenesis (Dixit *et al.*, 2014). Having now demonstrated a new role for Sst2 in receptor localization, we wanted to know how Sst2 affects the variability in this measure. To that end, we analyzed single-cell traces of Ste2-GFP at the plasma membrane over time (Supplemental Figure S1). Surprisingly, we found that fluctuations, defined as the coefficient of variation in fluorescence, did not follow the typical scaling behavior ($\sim 1/\text{mean}^{1/2}$) expected when only synthesis and degradation events are considered (Figure 5A; Kaern *et al.*, 2005). In addition, when the variance in fluorescence is plotted as a function of the mean, the data for wild-type cells and all the mutant strains collapse on a single curve (Figure 5B). Thus, whereas Sst2 suppresses noise in processes downstream of the receptor, it does not appear to affect

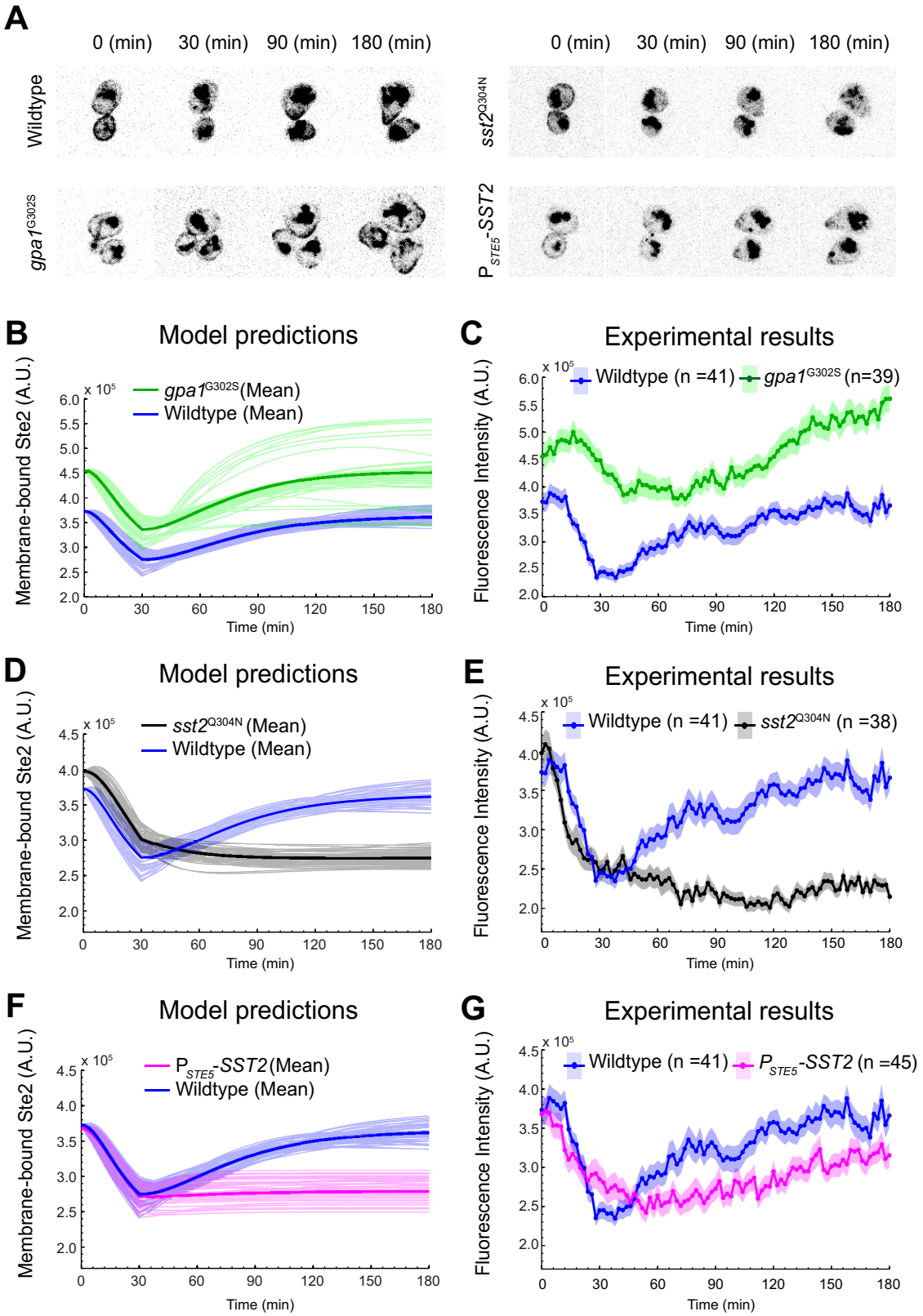

FIGURE 4: Model validation. (A) Representative fluorescence images of Ste2-GFP in *gpa1*^{G302S}, *sst2*^{Q304N}, and P_{STE5}-*SST2* strains treated with 150 nM pheromone. Wild-type results from Figure 1A are also shown for comparison. Black arrows indicate polarized receptor. (B) Model predictions for membrane-bound Ste2-GFP in the *gpa1*^{G302S} mutant. Individual predictions using the top 50 parameter sets are shown as thin green lines, and the mean of the top 50 time series is shown as a dark green line. For comparison, the WT results are replotted from Figure 2C (blue lines). (C) Experimental results for membrane-bound Ste2-GFP fluorescence in the *gpa1*^{G302S} mutant plotted as a function of time. The solid green line represents the mean, and the shaded green region shows the SE in the data. Cells were

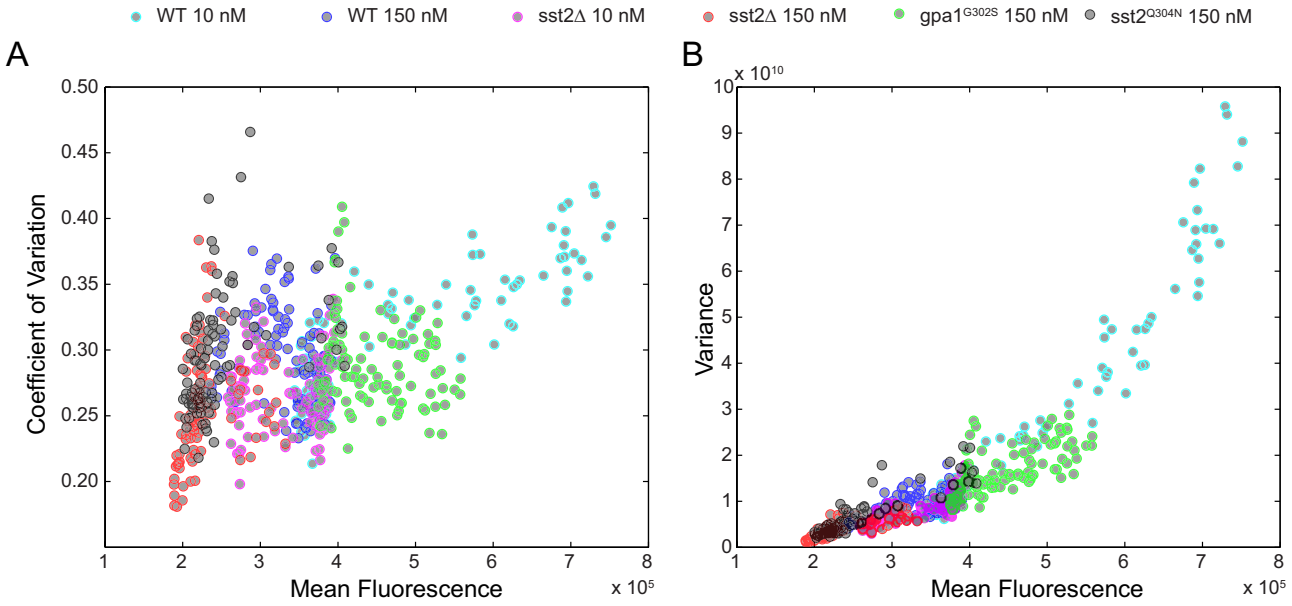

FIGURE 5: Cell-to-cell variability in receptor levels is not regulated by Sst2. (A) The coefficient of variation (SD/mean) for membrane-bound Ste2-GFP as a function of mean membrane-bound Ste2-GFP for each measured time point and each strain. (B) Same as in A, except for the variance vs. the mean.

noise at the level of the receptor. One possible explanation for our experimental observations is that the stochastic nature of vesicle delivery and fluctuations in the Ste2 abundance on the vesicles combine to generate the unexpected noise characteristics.

DISCUSSION

The primary functions of GPCRs are to translate external chemical gradients into internally polarized protein distributions and initiate intracellular signals that regulate gene expression. It seems reasonable to assume that each function brings with it a distinct set of operational requirements. Therefore it is evident that GPCR-mediated signaling is regulated by multiple control mechanisms that both promote and inhibit pathway activity. Consistent with this idea, our results demonstrate how a single protein, Sst2, which is known to limit G protein activity, also promotes receptor signaling. Specifically, we showed that the Sst2–receptor interaction, but not Sst2 GAP activity, is required for proper receptor recovery after pheromone stimulation. Central to our analysis were the *gpa1*^{G302S} and *sst2*^{Q304N} mutants. We showed previously that these mutants are, by at least four different measures, equally sensitive to pheromone stimulation (Dixit *et al.*, 2014). Thus the ability to separate the two known functions of Sst2 allowed us to assess the contributions of each binding interaction without the confounding effects of differences in signal output. Consequently we did not need to consider differences in Gβγ-dependent MAPK activation or new gene transcription, since these, too, are equivalent in the two mutants. This is important in light of evidence that Gβ phosphorylation is necessary for proper cell polarization (Zhu *et al.*, 2011) and gradient tracking (Deflorio *et al.*, 2013; Surve *et al.*, 2014). Thus the *gpa1*^{G302S} and *sst2*^{Q304N} mutants provide powerful experimental tools for dissecting the functional interactions of Sst2.

Our discovery that Sst2 is required for proper polarized recovery of the receptor after pheromone-induced receptor endocytosis adds to a growing list of roles for RGS proteins. For example, we recently demonstrated that Sst2 acts to suppress pathway noise (Dixit *et al.*, 2014). In this case, we used the *gpa1*^{G302S} and *sst2*^{Q304N} mutants to show that noise suppression requires Sst2 GAP activity but not its interaction with the receptor. RGS proteins have also been demonstrated to promote spatially focused signaling through a mechanism referred to as kinetic scaffolding (Zhong *et al.*, 2003). In kinetic scaffolding, increased GTP hydrolysis by RGS proteins promotes faster recoupling of the G protein to the receptor, generating strong localized signals.

To investigate the function of Sst2 binding to the receptor, we developed a mathematical model of Ste2 signaling and trafficking. A key assumption of the model was that Sst2 prevents receptor endocytosis by directly binding to the receptor. The key prediction of the model was that pheromone-induced increases in Sst2 abundance are required for proper receptor recovery. Through experimentation we validated three key predictions of the model: 1) Sst2 GAP activity is not required for receptor recovery, 2) Sst2 interaction with the receptor is required for receptor recovery, and 3) pheromone-dependent synthesis of Sst2 is required for receptor recovery.

To test the model, we used the mutant *gpa1*^{G302S}, which disrupts Sst2's interaction with the Gα subunit (DiBello *et al.*, 1998) and thus prevents Sst2 from accelerating GTP hydrolysis. Consistent with the

treated with 150 nM pheromone starting at 0 min. For comparison, the results for WT cells are replotted from Figure 1B (blue lines). (D) Model predictions for the *sst2*^{Q304N} mutant. Results are presented as described in B. (E) Experimental results for membrane-bound Ste2-GFP fluorescence in the *sst2*^{Q304N} mutant plotted as a function of time. Results are presented as described in C. (F) Model predictions for the P_{STE5}-*SST2* mutant. Results are presented as described in B. (G) Experimental results for membrane-bound Ste2-GFP fluorescence in the P_{STE5}-*SST2* mutant plotted as a function of time. Results are presented as described in C.

model's predictions, cells containing this mutant showed normal receptor recovery after pheromone-induced internalization. We then turned to the mutant *sst2*^{Q304N}, which disrupts Sst2 interaction with the receptor (Ballon *et al.*, 2006). Consistent with the model's predictions, this mutant did not show any receptor recovery. These results suggested that Sst2's interaction with the ligated receptor prevents receptor endocytosis. Finally, we validated the model by placing *SST2* under the control of a promoter that does not respond to pheromone. Consistent with the model's prediction, cells expressing constant levels of Sst2 did not recover to the level of WT cells, and the recovery that did occur was at a significantly slower rate. In addition to these explicit tests of the model, we asked whether Sst2 binding promotes variability in receptor abundance at the cell surface. Previously we demonstrated increased noise in transcription and cell morphogenesis in the *sst2*Δ and *gpa1*^{G302S} (but not in *sst2*^{Q304N}) cells. However, we found that the expression of Ste2-GFP was equally "noisy" in the four strains tested: *sst2*Δ, *sst2*^{Q304N}, *gpa1*^{G302S}, and WT cells. Thus, whereas interaction of Sst2 with Gpa1 reduces noise at the level of transcription and morphogenesis, interaction with the receptor does not promote variability in its expression at the plasma membrane. Taken together, our results establish a novel role for Sst2 in promoting receptor recovery at the growing edge of cells responding to pheromone.

Our finding that Sst2's GAP activity is dispensable for receptor recovery is in contrast to studies in neurons, which found that both the GAP and DEP domains of the RGS9-2 protein were needed to stabilize cell surface levels of D2-dopamine receptor (Celver *et al.*, 2010). There are differences between the yeast and neuronal systems that may account for this discrepancy. RGS9-2, in contrast to Sst2, has a Gγ-like domain and requires the expression of an atypical Gβ (Celver *et al.*, 2010). Although the details may differ from system to system, the broader regulatory features are likely to be conserved across species. Thus RGS proteins, which are well known as negative regulators of G protein signaling, also have a positive signaling function that is likely to modulate a variety of receptor pathways.

MATERIALS AND METHODS

Cell growth conditions and strain construction

Standard yeast media preparation, culture growth, and maintenance procedures were followed. All of the strains used in this study were made in the BY4741 background. Standard protocols for transformation of yeast and bacteria and manipulation of DNA were used. See the Supplemental Information for details of strain construction.

Live-cell imaging and microfluidics

Ste2 endocytosis was measured by monitoring the fluorescence of GFP-tagged Ste2 on the cell membrane after pheromone stimulation. Overnight starter cultures were diluted twice. The second dilution was made in 5 ml of synthetic complete medium with dextrose (SCD), and the cells were grown in an incubator shaker at 30°C until the OD_{600} reached 0.2. The live-cell imaging experiment was carried out in a microfluidic device described previously (Hao *et al.*, 2008). The microfluidic device is mounted on an Olympus (Tokyo, Japan) IX81 microscope with a Yokogawa Spinning Disk (Yokugawa Electric Corp., Tokyo, Japan) and Andor IXon Ultra EMCCD Camera (Andor Technology Ltd., Belfast, UK) for live-cell imaging. Stage positions to be monitored during the time course were set using an ASI PZ-2000 XYZ Series Automated stage with piezo *z*-axis top plate (Applied Scientific Instrumentation, Eugene, OR). Differential Inference Contrast (DIC) and fluorescence images were acquired at 2min intervals at 100× magnification using MetaMorph software (Molecular Devices, Sunnyvale, CA). DIC images were acquired using 100-ms exposure and an electron-multiplying (EM) gain of 2. GFP images were acquired using 400-ms exposure at 8% laser intensity (488-nm line of an argon laser) and an EM gain of 200. Image processing was done in ImageJ (National Institutes of Health, Bethesda, MD), and the quantification of Ste2 was performed in MATLAB (MathWorks, Natick, MA).

Quantification of membrane-bound Ste2 from fluorescence microscopy images

Raw DIC images from microscopy experiments were loaded into ImageJ. Cell boundaries were identified manually and saved in ImageJ ROI Manager. Raw fluorescence images from the same experiment were then loaded into ImageJ. The background fluorescence was subtracted using a standard background subtraction algorithm in ImageJ with a rolling ball radius of 150 pixels. The cell boundaries identified using DIC images were used to calculate Ste2 membrane intensity from fluorescence images. For each cell, an annular ring was created by shrinking the cell boundary (red line) by three pixels (cyan line; Figure 1B). The intensity of Ste2 on the cell membrane was calculated as the difference between intensities inside red and green circles in MATLAB. The time series of fluorescence intensities of membrane-bound Ste2 in each cell was plotted. Mean and SDs of all the single-cell time series were calculated to generate a mean fluorescence intensity profile of membrane-bound Ste2.

Single-cell traces of membrane-bound Ste2

The intensity of Ste2 on the cell membrane was calculated as described. The time series of fluorescence intensities of membrane-bound Ste2 in each cell was plotted. Each cell trace was represented in a different color. The mean of all the single-cell traces was plotted as a thick red line.

Comparison of Ste2-GFP in different strains at steady state

Measured Ste2-GFP fluorescence varies with day-to-day fluctuations in the laser intensity. To compare Ste2-GFP fluorescence across different strains, we sought to normalize the fluctuations in laser intensity between experiments done on different days by measuring steady-state Ste2-GFP fluorescence in cells simultaneously. The cells were grown in an incubator shaker at 30°C until the OD_{600} reached 0.2 as described under *Live-cell imaging and microfluidics*. A 10-μl amount of cells was plated on 2% agarose pads and covered with a Corning (Corning, NY) microscope cover glass. The agar pads were mounted on the Olympus microscope described earlier, and fluorescence images were acquired at 100× magnification using MetaMorph software. Background subtraction and cell boundary identification was done in ImageJ, and annular rings of 3-pixel width were created. The amount of Ste2-GFP on the membrane was measured as the fluorescence intensity in the annular rings. A box plot was created for membrane-bound Ste2-GFP levels measured for each strain. Because the cells were not treated with pheromone, the box plot thus created is a measure of the steady-state Ste2-GFP in the strains. Student's *t* test was conducted to confirm that the steady-state receptor levels in different strains were significantly different from those in the WT strain. Mean steady-state Ste2-GFP levels and *p* values from Student's *t* test are reported in the Supplemental Information.

Receptor distribution

The distribution of Ste2-GFP on the mating projection was measured using FIJI by drawing a line encompassing the polarized receptor across the mating projection. To avoid obscuring the signal from plasma membrane–associated Ste2, we analyzed only those

cells that did not have a vacuolar or endosomal signal coincident with the polarized edge of the cell (Supplemental Figure S2A). The resultant line scans were analyzed in MATLAB. The Ste2 profiles were smoothed (MATLAB "smooth" function, span of 20 pixels), and the maximum of the smoothed profile was used to determine the center of the receptor distribution. The raw data from each cell were then spatially aligned to the center of the distribution (Supplemental Figure S2B), and then all cells were averaged. The minimum value from the average profile was subtracted, as it represented the background intensity on the membrane, and the profile was normalized to sum to 1. The average values are shown as circles, and the line shows the average values smoothed (as before, span of 3).

Mathematical modeling

We developed two mathematical models to investigate the role of Sst2 in regulating endocytosis of the receptor Ste2 after pheromone treatment. The models are based on ordinary differential equations and take the pheromone concentration as input and compute the time course of Ste2 abundance. The model that does not account for Sst2's interaction with the receptor consists of eight coupled ordinary differential equations (ODEs) and 30 parameters. The expanded model consists of 10 coupled ODEs and 32 parameters. Both models were solved using the ode15s solver in MATLAB. See the Supplemental Information for the model equations and parameter descriptions and values.

Parameter estimation

Parameter estimation was performed using a modified evolutionary algorithm as described previously (Fu *et al.*, 2014). The model was trained with Ste2-GFP time course data for wild-type and *sst2*Δ cells treated with 150 nM pheromone. Twelve instances of the algorithm were run in parallel, each starting with six different sets of parent parameter values. Half of the initial parent parameter sets were estimated from the literature, and the remaining half were chosen randomly. In the algorithm, p was set to 6, $C = 6$, $\mu = 30\%$, $\lambda = 10\%$, and $\beta = 1.5$. The algorithm was run for 3000 generations, which resulted in 1.3 million trials in the parameter search. The top 50 scored parameter sets were used to compare remaining data sets and make testable predictions. See the Supplemental Information for the parameter estimation results.

ACKNOWLEDGMENTS

We thank Daniel Lew for valuable comments on the manuscript. This work was supported by National Institutes of Health Grants GM080739 (H.D.), GM103870 (T.E.), GM079271 (T.E. and B.E.), and GM114136 (T.E., B.E., and H.D.) and American Heart Association postdoctoral fellowship 11POST7600017 (J.K.).

REFERENCES

Apanovitch DM, Slep KC, Sigler PB, Dohlman HG (1998). Sst2 Is a GTPase-activating protein for Gpa1: purification and characterization of a cognate RGS–Gα protein pair in yeast†. Biochemistry 37, 4815–4822.

Ballon DR, Flanary PL, Gladue DP, Konopka JB, Dohlman HG, Thorner J (2006). DEP-domain-mediated regulation of GPCR signaling responses. Cell 126, 1079–1093.

Celver J, Sharma M, Kovoor A (2010). RGS9-2 mediates specific inhibition of agonist-induced internalization of D2-dopamine receptors. J Neurochem 114, 739–749.

Chen Q, Konopka JB (1996). Regulation of the G-protein-coupled alpha-factor pheromone receptor by phosphorylation. Mol Cell Biol 16, 247–257.

Deflorio R, Brett ME, Waszczak N, Apollinari E, Metodiev MV, Dubrovskyi O, Eddington D, Arkowitz RA, Stone DE (2013). Phosphorylation of Gbeta is crucial for efficient chemotropism in yeast. J Cell Sci 126, 2997–3009.

DiBello PR, Garrison TR, Apanovitch DM, Hoffman G, Shuey DJ, Mason K, Cockett MI, Dohlman HG (1998). Selective uncoupling of RGS action by a single point mutation in the G protein alpha-subunit. J Biol Chem 273, 5780–5784.

Dixit G, Kelley JB, Houser JR, Elston TC, Dohlman HG (2014). Cellular noise suppression by the regulator of G protein signaling Sst2. Mol Cell 55, 85–96.

Dohlman HG, Song J, Ma D, Courchesne WE, Thorner J (1996). Sst2, a negative regulator of pheromone signaling in the yeast Saccharomyces cerevisiae: expression, localization, and genetic interaction and physical association with Gpa1 (the G-protein alpha subunit). Mol Cell Biol 16, 5194–5209.

Dohlman H, Thorner J (2001). Regulation of G protein-initiated signal transduction in yeast: paradigms and principles. Annu Rev Biochem 70, 703–754.

Doncic A, Falleur-Fettig M, Skotheim JM (2011). Distinct interactions select and maintain a specific cell fate. Mol Cell 43, 528–539.

Dyer JM, Savage NS, Jin M, Zyla TR, Elston TC, Lew DJ (2013). Tracking shallow chemical gradients by actin-driven wandering of the polarization site. Curr Biol 23, 32–41.

Flotho A, Simpson DM, Qi M, Elion EA (2004). Localized feedback phosphorylation of Ste5p scaffold by associated MAPK cascade. J Biol Chem 279, 47391–47401.

Fu Y, Lim S, Urano D, Tunc-Ozdemir M, Phan NG, Elston TC, Jones AM (2014). Reciprocal encoding of signal intensity and duration in a glucose-sensing circuit. Cell 156, 1084–1095.

Hague C, Bernstein LS, Ramineni S, Chen Z, Minneman KP, Hepler JR (2005). Selective inhibition of alpha1A-adrenergic receptor signaling by RGS2 association with the receptor third intracellular loop. J Biol Chem 280, 27289–27295.

Hao N, Nayak S, Behar M, Shanks RH, Nagiec MJ, Errede B, Hasty J, Elston TC, Dohlman HG (2008). Regulation of cell signaling dynamics by the protein kinase-scaffold Ste5. Mol Cell 30, 649–656.

Howell AS, Jin M, Wu CF, Zyla TR, Elston TC, Lew DJ (2012). Negative feedback enhances robustness in the yeast polarity establishment circuit. Cell 149, 322–333.

Jenness DD, Spatrick P (1986). Down regulation of the α-factor pheromone receptor in S. cerevisiae. Cell 46, 345–353.

Jin M, Errede B, Behar M, Mather W, Nayak S, Hasty J, Dohlman HG, Elston TC (2011). Yeast dynamically modify their environment to achieve better mating efficiency. Sci Signal 4, ra54.

Kaern M, Elston TC, Blake WJ, Collins JJ (2005). Stochasticity in gene expression: from theories to phenotypes. Nat Rev Genet 6, 451–464.

Kelley JB, Dixit G, Sheetz JB, Venkatapurapu SP, Elston TC, Dohlman HG (2015). RGS proteins and septins cooperate to promote chemotropism by regulating polar cap mobility. Curr Biol 25, 275–285.

Konopka JB, Jenness DD, Hartwell LH (1988). The C-terminus of the S. cerevisiae alpha-pheromone receptor mediates an adaptive response to pheromone. Cell 54, 609–620.

Kovoor A, Seyffarth P, Ebert J, Barghshoon S, Chen C-K, Schwarz S, Axelrod JD, Cheyette BNR, Simon MI, Lester HA, Schwarz J (2005). D2 dopamine receptors colocalize regulator of G-protein signaling 9–2 (RGS9-2) via the RGS9 DEP domain, and RGS9 knock-out mice develop dyskinesias associated with dopamine pathways. J Neurosci 25, 2157–2165.

Neubig RR, Siderovski DP (2002). Regulators of G-protein signalling as new central nervous system drug targets. Nat Rev Drug Discov 1, 187–197.

Parnell SC, Marotti LA, Kiang L, Torres MP, Borchers CH, Dohlman HG (2005). Phosphorylation of the RGS protein Sst2 by the MAP kinase Fus3 and use of Sst2 as a Model To analyze determinants of substrate sequence specificity. Biochemistry 44, 8159–8166.

Reneke JE, Blumer KJ, Courchesne WE, Thorner J (1988). The carboxy-terminal segment of the yeast alpha-factor receptor is a regulatory domain. Cell 55, 221–234.

Schandel KA, Jenness DD (1994). Direct evidence for ligand-induced internalization of the yeast alpha-factor pheromone receptor. Mol Cell Biol 14, 7245–7255.

Segall JE (1993). Polarization of yeast cells in spatial gradients of alpha mating factor. Proc Natl Acad Sci USA 90, 8332–8336.

Shintani T, Klionsky DJ (2004). Cargo proteins facilitate the formation of transport vesicles in the cytoplasm to vacuole targeting pathway. J Biol Chem 279, 29889–29894.
Sjögren B, Blazer LL, Neubig RR (2010). Prog Mol Biol Transl Sci 91, 81–119.
Sprang SR (1997). G protein mechanisms: insights from structural analysis. Annu Rev Biochem 66, 639–678.
Suchkov DV, DeFlorio R, Draper E, Ismael A, Sukumar M, Arkowitz R, Stone DE (2010). Polarization of the yeast pheromone receptor requires its internalization but not actin-dependent secretion. Mol Biol Cell 21, 1737–1752.
Surve CR, Lehmann D, Smrcka AV (2014). A chemical biology approach demonstrates G protein betagamma subunits are sufficient to mediate directional neutrophil chemotaxis. J Biol Chem 289, 17791–17801.
Yildirim N, Hao N, Dohlman HG, Elston TC (2004). Mathematical modeling of RGS and G- protein regulation in yeast. Methods Enzymol 389, 383–398.
Yu RC, Pesce CG, Colman-Lerner A, Lok L, Pincus D, Serra E, Holl M, Benjamin K, Gordon A, Brent R (2008). Negative feedback that improves information transmission in yeast signalling. Nature 456, 755–761.
Zanolari B, Raths S, Singer-Kruger B, Riezman H (1992). Yeast pheromone receptor endocytosis and hyperphosphorylation are independent of G protein-mediated signal transduction. Cell 71, 755–763.
Zhang P, Mende U (2011). Regulators of G-protein signaling in the heart and their potential as therapeutic targets. Circ Res 109, 320–333.
Zhong H, Wade SM, Woolf PJ, Linderman JJ, Traynor JR, Neubig RR (2003). A spatial focusing model for G protein signals. Regulator of G protein signaling (RGS) protein-mediated kinetic scaffolding. J Biol Chem 278, 7278–7284.
Zhu M, Torres MP, Kelley JB, Dohlman HG, Wang Y (2011). Pheromone- and RSP5-dependent ubiquitination of the G protein beta subunit Ste4 in yeast. J Biol Chem 286, 27147–27155.